IN-07

027252

NASA Technical Memorandum 107450
AIAA–97–2486

Heat Transfer Computations of Internal Duct Flows With Combined Hydraulic and Thermal Developing Length

C.R. Wang, C.E. Towne, S.A. Hippensteele, and P.E. Poinsatte
Lewis Research Center
Cleveland, Ohio

Prepared for the
32nd Thermophysics Conference
sponsored by the American Institute of Aeronautics and Astronautics
Atlanta, Georgia, June 23–25, 1997

National Aeronautics and
Space Administration

HEAT TRANSFER COMPUTATIONS OF INTERNAL DUCT FLOWS WITH COMBINED HYDRAULIC AND THERMAL DEVELOPING LENGTH

C.R. Wang, C.E. Towne, S.A. Hippensteele, and P.E. Poinsatte
National Aeronautics and Space Adminsitration
Lewis Research Center
Cleveland, Ohio 44135

Abstract

This study investigated the Navier-Stokes computations of the surface heat transfer coefficients of a transition duct flow. A transition duct from an axisymmetric cross section to a nonaxisymmetric cross section, is usually used to connect the turbine exit to the nozzle. As the gas turbine inlet temperature increases, the transition duct is subjected to the high temperature at the gas turbine exit. The transition duct flow has combined development of hydraulic and thermal entry length. The design of the transition duct required accurate surface heat transfer coefficients. The Navier-Stokes computational method could be used to predict the surface heat transfer coefficients of a transition duct flow. The Proteus three-dimensional Navier-Stokes numerical computational code was used in this study. The code was first studied for the computations of the turbulent developing flow properties within a circular duct and a square duct. The code was then used to compute the turbulent flow properties of a transition duct flow. The computational results of the surface pressure, the skin friction factor, and the surface heat transfer coefficient were described and compared with their values obtained from theoretical analyses or experiments. The comparison showed that the Navier-Stokes computation could predict approximately the surface heat transfer coefficients of a transition duct flow.

Nomenclatures

C_f	skin friction factor, $\tau_w/(1/2\ \rho_\infty U_\infty^2)$
D	hydraulic diameter
H	heat transfer coefficient, $Q_w/(T_w - T_\infty)$, Btu/(hr-ft^2 °R)
h	dimensionless heat transfer coefficient, HR/K
K	heat conductivity
k	turbulence kinetic energy
L	domain along X-direction
n	normal direction
Pr	Prandtl number, 0.71
p	static pressure
Q_w	heat transfer rate
R	circular duct radius
Re_b	bulk Reynolds number, $\rho_\infty U_\infty D/\mu_\infty$
T	temperature
U,V,W	velocity components
X,Y,Z	Cartisian coordinates
X,r,θ	cylindrical coordinates
Y^+	dimensionless distance from wall surface, $n\sqrt{\tau_w \rho_w}/\mu_w$
β_X,β_Y,β_Z	grid packing parameters
ε	turbulence kinetic energy dissipation rate
τ_w	shear stress

Subscripts

c	center-line condition
d	downstream location
s,w	surface/wall condition

u	upstream inlet location
∞	inlet condition
o,∞	inlet stagnation condition

Introduction

Nonaxisymmetric exhaust nozzles are often employed on the modern aircraft propulsion systems to improve the aircraft performance. A transition duct, from an axisymmetric cross section to a nonaxisymmetric cross section, is needed to connect the turbine exit to the nozzle. In applications, the incoming flow to the transition duct is turbulent and subsonic. Existing research[1,2] has experimentally explored the aerodynamics of a circular to rectangular transition duct flow. Their emphases were on the measurements of the total pressure and the shear stresses. As the gas turbine inlet temperature increases, the transition duct is subjected to the high temperature at the gas turbine exit. The transition duct flow has combined development of hydraulic and thermal entry length. The temperature distribution along the duct surface is an important factor in the design of the transition duct. The attainment of the duct surface temperature requires the accurate predictions of the surface heat transfer coefficients.

A method of using a liquid crystal-heater composite sheet for heat transfer research was developed at the NASA Lewis Research Center.[3,4] The method was successful to resolve the heat transfer coefficients of a square to rectangular transition duct flow.[5] Recently, this method was used to measure the heat transfer coefficients of a circular to rectangular transition duct flow.[6]

Numerical computational methods of the Navier-Stokes equations and the energy equation could be used to compute the velocity and the temperature variations within a flow field. Using the advanced computational grid generation technique, such as the Gridgen Routines,[7] one could optimize the computational grid for complicated flow geometries such as the internal flows within transition ducts. The turbulence modeling technique has also been improved[8] for the Navier-Stokes computations of turbulent flows. With proper turbulence model and computational grid in the Navier-Stokes computation, it could be used to compute the temperature variation within the near wall region of a turbulent transition duct flow. Based on the near wall temperature variations, we could calculate the surface heat transfer coefficients.

The objective of this study was to investigate the capability of the Navier-Stokes code to predict the heat transfer coefficients at the wall surface of an experimental transition duct.[1] The transition duct, Fig. 1, changed its circular cross section at the upstream locations to rectangular cross section at the downstream locations. The axis of the duct was in line with the upstream flow direction. The upstream flow was turbulent and had a Mach number of 0.34. The Reynolds number of the upstream flow was 1.6×10^6. The Proteus three-dimensional Navier-Stokes numerical computational code[9] was used for the present computational study. The Gridgen software program was used to generate the computational grid. The unsteady, compressible, and turbulent Reynolds averaged Navier-Stokes equations and the energy equation were solved numerically for the steady state flow properties of the transition duct flow.

In this report, we describe a preliminary study of using the Proteus code to predict the heat transfer coefficients of the transition duct flow. The code was first studied for its capabilities to calculate the turbulent internal flow properties of a circular duct and a square duct. These served as baseline verifications of the computational code. The code was then used to compute the properties of the transition duct flow. The computed heat transfer coefficients were compared with their measurements to investigate the capability of Navier-Stokes computation of the transition duct surface heat transfer coefficients.

Computation

The Proteus Navier-Stokes numerical computational code was used in this study. The theory, the numerical schemes, and the usage of the code could be found in Refs. 9 to 11. The code solved the unsteady, compressible Reynolds-averaged Navier-Stokes equations and energy equation for turbulent flow properties. The Baldwin-Lomax eddy viscosity formula[12] and the Chien's k-ε turbulence model[13] were coded for turbulence modeling. The code solved the governing equations in either the Cartesian or the cylindrical coordinate systems. The equations were solved by marching in time using the generalized time differencing of Beam and Warming.[14] The second order central differencing was used for all spatial derivatives. Nonlinear terms were linearized using second-order Taylor series expansions. The finite difference equations were solved using an alternating-direction-implicit technique.[15] A set of coordinates to specify the computational grid was required for a particular flow geometry. These coordinates could be created by a separate grid generation code and stored in an unformatted file for the Proteus code to read. A variety of the boundary conditions of mean velocity components, temperature, pressure and turbulence for the computations were built into the code including (1) specified values and/or gradients, and (2) linear extrapolation. Thus, the Proteus Navier-Stokes code was suitable for the present heat transfer computations of the internal duct flows with combined development of hydraulic and thermal entry length.

In this study, the Proteus code was used to calculate respectively the properties of the developing turbulent flows within (a) a circular duct, (b) a square duct and (c) a circular to rectangular transition duct. The present computation used most of the default numerical computational schemes in the existing code. The second derivative viscous terms were included in the computation and it did not use the thin-layer option. The computations also included the constant coefficient models of fourth-order explicit artificial viscosity and second-order implicit artificial viscosity. The coefficients were all 1.0 for the fourth-order viscosity model and all 2.0 for the second-order viscosity model. The Euler implicit method and a local time step based on the CFL criteria for explicit method were utilized in the computations. A CFL value of 10 was used in the computation with the Baldwin-Lomax eddy viscosity formula for turbulence modeling. A small CFL value of 1 was used in the computation with the Chien's k-ε two-equation model for turbulence modeling. The convergence was based on the averaged absolute value of the residual for each conservation equation. The convergence was assumed when the maximum residual was less than 4×10^{-6}. The boundary conditions and the initial conditions were specified for each internal duct flow computations. The effect of the computational grid and the turbulence model on the computations were first studied in the circular duct flow and the square duct flow computations. These computations were served as the code verifications. The code was then used to compute the transition duct flow surface heat transfer coefficients with selected grid configurations and turbulence model. The grid configurations, the initial conditions, the boundary conditions and the turbulence model for each flow computation were described in the following section.

Circular Duct Flow

The hydrodynamics and thermodynamics of a circular duct flow is often used to simulate the internal flow properties of noncircular duct. However, existing heat transfer studies of a circular duct flow[16] are limited to the case with a fully-developed velocity profile condition. In practice, the hydrodynamics and thermodynamics flow fields developed simultaneously in the inlet region. The computation of the heat transfer properties of the developing circular duct flow was considered here. Figure 2 shows a sketch of the flow configuration. The duct has a constant circular cross section with a radius of R = 0.36 ft. We used the cylindrical coordinate system for the computation.

Boundary Conditions. To simulate the flow field with combined hydraulic and thermal entry length, uniform mean velocity and mean temperature were assigned to be the boundary conditions at X/R = 0. Near the duct inlet (X/R = 0), the static pressure was assumed to vary linearly along the X-direction. The downstream boundary of the computational domain was chosen to be at X/R = 100 (L = 100R). A fully developed flow existed[17] near the downstream boundary location. Thus, the X-direction gradients of the mean velocity components and the static temperature were zero at X/R = 100 location. Uniform static pressure was specified at the downstream boundary locations. The computations were performed within a quadrant of the duct geometry and symmetric boundary conditions were assigned at $\theta = 0°$ and $\theta = 90°$ locations. The r-direction gradients of the flow properties were zero at the duct center line locations. Nonslip conditions were the velocity boundary conditions at the duct wall surface. The normal pressure gradient was set to zero at the duct wall surface. The duct wall surface temperature was assumed to be uniform and had a value of $1.1\ T_\infty$.

The Baldwin-Lomax eddy viscosity formula was used for turbulence modeling in the computation. This algebraic turbulence model was modified for an internal duct flow computations.[9] This turbulence model does not require the turbulence boundary conditions for its usage in the computation.

Computational Grids. The grid dimensions were 81 along the X-direction, 31 along the θ-direction, and 50 along the r-direction. The grid points at each X location were located in the duct cross section. The grid configuration was kept the same at every duct cross section. The following equation,

$$X/L = (\beta_x + 1) - (\beta_x - 1)\left\{\left[(\beta_x + 1)/(\beta_x - 1)\right]^{1-\bar{x}}\right\} \Big/ \left\{\left[(\beta_x + 1)/(\beta_x - 1)\right]^{1-\bar{x}} + 1\right\} \quad (1)$$

with $0 \le \bar{x} < 1$ and $\beta_x \doteq 1$, was used to distribute the grid points along the X-direction. Three different grids ($\beta_x = 1.0$, 1.01 or 1.05) were considered respectively in the computations.

Within each duct cross section, the grid points were uniformly distributed along the θ-direction. Along the r-direction, the grid points were packed at the near duct wall locations (There were five grid points in $Y^+ < 10$ at the downstream location and the first grid point from the surface was at $Y^+ = 0.79$). Since we did not change the grid point distribution within each duct cross section, we only considered the effect of the X-directional grid packing on the computation.

Initial Conditions. The inlet free stream properties were used as the initial conditions at each grid point to start the time iterations. The free stream had a total pressure 14.7 psia, a total temperature of 520 °R, and a Mach number of 0.34. These free stream conditions gave a bulk Reynolds number $Re_b = 1.6\times10^6$. The Baldwin-Lomax eddy viscosity formula was used for turbulence modeling. The computation did not require turbulence initial conditions.

Square Duct Flow

A sketch of the flow configuration was shown in Fig. 3. We used the Cartesian coordinate system in the computation. The duct axis was in line with the inlet flow direction and the shape of the duct cross section did not change along the axial direction. Gessner[18] measured the flow properties within the near wall region. These existing experimental results could be used to verify the accuracy of the Navier-Stokes computations. The present computation was intended to predict some of the experimental results with bulk Reynolds number, $Re_b = 2.5\times10^5$. The existing experimental results indicated that the flow would be fully developed at X/D = 80. Thus, the computational domain was chosen to be a quadrant of the duct between X/D = 0 and X/D = 80.

Boundary Conditions. Uniform velocity and uniform temperature were assumed at the duct inlet to simulate the flow with combined development of the hydraulic and thermal entry length. Near the duct inlet, the static pressure was assumed to vary linearly along the X-direction. Nonslip velocity conditions were the boundary conditions at the duct wall surface. The wall surface temperature was assumed to be uniform and the temperature was set at 1.1 T_∞. The normal pressure gradients at the wall surface were set to zero. The flow symmetric conditions were the boundary conditions along the boundary at Y = D/2 and Z = D/2. Within the downstream duct cross-section (at X/D = 80), the X-direction gradients of the mean velocity components and the mean temperature were zero. They were the boundary conditions. However, a X-direction pressure gradient was imposed at the downstream location (X/D = 80). This pressure gradient was estimated according to the theoretical analysis[17] and the measurements of wall stresses.[18]

The Baldwin-Lomax eddy viscosity model and the Chien's k-ε turbulence model were studied respectively for the turbulence modeling in the computation. For the k and ε computations, the gradients of k and ε were set to zero at the upstream and the downstream boundaries. Noslip boundary conditions (k = 0 and ε = 0) were used at the duct wall surface. Symmetry conditions were used at the planes of symmetry.

Computational Grids. The grid dimensions were chosen to be 100 along the X-direction, 40 along the Y-direction, and 40 along the Z-direction. The grid generation technique in Ref. 10 was used to pack the grid points at the locations near the duct inlet and the duct wall surface. The grid point spacing along the X, Y, and Z directions were adjusted by specifying the packing parameters β_X, β_Y and β_Z. To study the grid effect on the computation, two different grids were used respectively to perform similar flow computations.

One grid was generated with $\beta_X = 1.1$, $\beta_Y = \beta_Z = 1.0075$. The grid points were sparsely distributed at the near wall surface locations (There were 3 grid points in $Y^+ < 10$ at X/D = 80, Z/D = 0.5 and the first grid point from the surface was at $Y^+ = 5.57$). This grid was used in two similar computations with either the Baldwin-Lomax eddy viscosity formula or the Chien's k and ε equations for turbulence modeling. Another grid was generated with $\beta_X = 1.1$, and $\beta_Y = \beta_Z = 1.002$ to increase the grid points in the near surface region (There were 5 grid points in $Y^+ < 10$ at X/D = 80, Z/D = 0.5 and the first grid point from the surface was at $Y^+ = 1.84$). This grid was used in the computation only with the Baldwin-Lomax eddy viscosity formula for turbulence modeling.

Initial Conditions. We used two different turbulence modeling techniques in the square duct flow computations. Different initial conditions, corresponding to different turbulence modeling techniques, were used to start the time iterations.

When the Baldwin-Lomax eddy viscosity formula was used in the computation, it used the upstream free stream properties as the initial conditions at each grid point location. The computed flow properties were the initial conditions for the square duct flow computation with the k-ε turbulence model. The Proteus code could generate[10] the initial k and ε conditions.

Circular to Rectangular Transition Duct Flow

A sketch of the duct flow configuration was shown in Fig. 4. Details of the duct geometry and its setup in the wind tunnel experiment could be found in Ref. 1. We did not consider the actual shape of the wind tunnel inlet in the present computation. However, the circular section was extended upstream in the present computation. The extension was to account for the effect of the wind tunnel inlet shape on the flow development. For the present computation, the duct geometry consisted of an upstream circular section, a transition mid section, and a downstream rectangular section. The radius of the circular section was 0.36 ft. The duct axis was in line with the inlet flow direction. The inlet flow had a Mach Number of 0.34, a total temperature of 520 °R and a total pressure of 14.7 psia. These flow conditions gave a bulk Reynolds number, $Re = 1.6\times10^6$. We used the cylindrical coordinate system for the computation.

Boundary Conditions. The computational domain was a quadrant of the duct between X/R = –6 and X/R = 7. The boundary conditions were specified at the inlet, the duct surface, the symmetric plans, the duct center line, and the downstream boundary of the domain of computation. The boundary conditions were similar to what were previously described for the circular duct flow computation. A summary of the boundary conditions were described mathematically in the following:

At the inlet location, $X/R = -6$, $dp/dX = 0$, $U = U_\infty$, $V = 0$, $W = 0$, and $T = T_\infty$. At the radial location, $0 < r < R$, along $\theta = 0°$ direction, $dp/d\theta = 0$, $dU/d\theta = 0$, $V = 0$, $dW/d\theta = 0$, and $dT/d\theta = 0$. At the radial location, $0 < r < R$, along $= 90°$ direction, $dp/d\theta = 0$, $dU/d\theta = 0$, $dV/d\theta = 0$, $W = 0$, and $dT/d\theta = 0$. At the location with $r = 0$ and $0° < \theta < 90°$, $dp/dr = 0$, $dU/dr = 0$, $dv/dr = 0$, $dW/dr = 0$, and $dT/dr = 0$. At the location with $r = R$ and $0° < \theta < 90°$, $dp/dn = 0$, $U = 0$, $V = 0$, $W = 0$, and $T = Tw$. At the downstream boundary location, $X/R = 7$, $p/p_\infty = 0.985$, $dU/dX = 0$, $dV/dX = 0$, $dW/dX = 0$, and $dT/dX = 0$.

The downstream static pressure boundary condition ($p/p_\infty = 0.985$) was chosen from the experimental results.[1] The purpose of the computation was to predict the surface heat transfer coefficients. Therefore, the surface temperature of the experiment[6] was used as the surface temperature boundary condition at $r = R$. The experiment imposed a step increase in the wall surface temperature along the X-direction and the surface temperature was uniform along the θ-direction. Thus, the surface temperature boundary conditions for the present computation were

$T_w = T_{0,\infty}$, for $X/D < -4$,

and

$T_w = 1.197T_\infty$, for $X/D \geq -4$.

Computational Grids. The computations were performed with two different grids in order to study the grid effect on the computation. The Gridgen program[7] was used to generate the grids. The grids had the same dimensions. The dimensions were 81 along the X-direction, 50 along the r-direction, and 31 along the θ-direction. The upstream circular section and the transition mid section, respectively, had 31*50*31 grid points. The downstream rectangular section had 21*50*31 grid points. Additional details of each grid were briefly described in the following sections.

First Grid. The grid point spacing along the axial direction was uniformly distributed within each of the three different duct sections. Within a duct cross section, the grid points were packed at near duct surface locations (the grid point spacing was approximately the same as that of the circular duct flow computation). The grid point were uniformly distributed ($\Delta\theta$ = constant) along the θ-direction. Thus the grid orthogonality at the duct surface was maintained within the upstream circular section and along the side wall and the top wall center lines of the transition mid section and the downstream rectangular section.

Second Grid. In the upstream circular section, the grid points fell on the duct cross sections. The grid points along the X-direction were packed at the locations near the duct entrance. Within each cross section, the grid points along the r-direction were packed at the locations near the duct axis and the duct wall surface (the near surface grid point spacing was approximately the same as that of grid 1). At the same r location, the grid points were uniformly distributed in the θ-direction. Within the transition mid section, the grid orthogonality at the locations near the wall surface was optimized with Gridgen routines. The grid points were packed at the locations near the duct axis and the duct wall surface. Within the downstream rectangular section, the grid points fell on the duct cross sections. The grid points were equally spaced along the X-direction. The grid configuration within each cross section was the same as that at the downstream side ($X/R = 3.75$) of the transition mid section.

Turbulence models. The Baldwin-Lomax eddy viscosity model was found effective (see the Results and Discussions section) for the computations of the internal flows within the circular duct and the square duct. This turbulence modeling technique was used for the circular to rectangular duct flow computation.

Initial Conditions. The Proteus code was previously used to compute the turbulent developing circular duct flow properties. The computed circular duct flow properties were the initial conditions for the computation of the circular to rectangular duct flow. The Baldwin-Lomax eddy viscosity formula was used for turbulence modeling and the computation did not require turbulence initial conditions.

Results and Discussions

The previously described computational conditions were implemented to the Proteus computational code. The computations were proceeded to calculate the properties of the developing flows within the circular duct, the square duct and the circular to rectangular transition duct. The experience from the numerical computations indicated that the CFL value affected the starting of the computation. When the computation used the Baldwin-Lomax eddy viscosity, it could be started with a large CFL value (CFl = 10 was used here). A small CFL value (= 1) was required to proceed the computation when Chien's k-ε turbulence model was used in the computation. The computations converged within 45,000 time iterations. Some of the computed flow parameters, such as the duct center-line velocity, the surface pressure, the skin friction factor and the surface heat transfer coefficient for each duct flow were described and compared with their values from theoretical analysis or experiments in the following sections.

Circular Duct Flow

For a developing cylindrical duct flow, the flow could be fully developed at downstream locations, $X/R > 80$.[17] The present computational domain, L/R, along the X-direction was chosen to be either 100 or 140. The static pressure was also imposed as a boundary condition at the downstream location. The downstream pressure could be different at different L/R locations. The present computation was repeated with a few combinations of the domain configuration and the downstream pressure value. We investigated the effect of the domain and the downstream static pressure on the computation.

A summary of the results of the X-directional variations of the center-line mean velocity, U_c/U_∞, were shown in Fig. 5. The existing measurements of U_c/U_∞ from experiment[17] were also plotted in Fig. 5 to compare with the present computed U_c/U_∞ values. Different grid point packings (β_x = 1.00, 1.01 or 1.05) along the X-direction did not affect the U_c/U_∞ computation. A slight increase in the downstream pressure value (from 0.945 to 0.960) did not change significantly the U_c/U_∞ computations. With $\beta_x = 1.05$, $p_d = 0.945p_\infty$ and different domain sizes (L/R = 100 or 140), the computations calculated approximately the same U_c/U_∞ variations along the X-direction. All the computed U_c/U_∞ values at near inlet locations ($X/R < 30$) agreed very well with the existing measurements. However, the computed U_c/U_∞ values at $X/R > 30$ locations were found to be larger than their measured values.

The computational results of the X-directional variations of the center-line static pressure, p_c/p_∞, were plotted in Fig. 6. The results showed that different static pressure level was computed when different computational domain or different downstream static pressure value was used in the computation. With L/R = 140 or $p_d/p_\infty = 0.960$ in the computation, it predicted an increase in the center-line static pressure within the entire duct flow region. The results showed that the static pressure varied linearly along the X-direction.

The computational results of the skin friction factor, C_f, were plotted in Fig. 7. The experimental results of the skin friction factors[17] were shown in this figure for comparison. Regardless of the difference in grid point packing, the computed skin friction factors at the near inlet locations ($X/R < 30$) agreed with the experimental values. The C_f value decreased from a large value at the duct inlet to a small value at $X/R = 30$ location and then C_f increased slightly at large X/R locations. When uniform grid point spacing ($\beta_x = 1$) was used in the computation, the computed C_f values oscillated at the downstream locations ($X/R > 50$). The computed C_f values were well correlated in term of X/R. The skin friction factor of fully developed turbulent circular duct flow was correlated[17] in term of the bulk Reynolds number,

$$C_f = \left[4\log_{10}\left\{Re_b/(4.53\log_{10}Re_b - 3.82)\right\}\right]^{-2} \qquad (2)$$

The present duct flow had a bulk Reynolds number, $Re_b = 1.6\times10^6$. Equation (2) predicted $C_f = 2.70\times10^{-3}$ for a fully developed flow. This skin friction factor value was also shown in Fig. 7 and compared with the present computational results of the downstream skin friction factors. The present computations predicted higher downstream skin friction factor value than it was computed with Eq. (2).

The computed surface heat transfer coefficients, h, were plotted in Fig. 8. The heat transfer coefficient was large at the duct inlet location and the h value decreased gradually at the downstream locations. The size of the domain of computation and the downstream static pressure value seemed to have little effect on the computation of the surface heat transfer coefficient. However, the computed h values at the downstream locations oscillated when the grid points were distributed uniformly ($\beta_x = 1$) along the X-direction. The h values were well correlated in term of X/R values. It was established[16] that the Nusselt number, Nu (= HD/K), and the bulk Reynolds number of a fully developed turbulent circular duct flow were correlated with

$$Nu = 0.021\,Pr^{0.6}\,Re_b^{0.8}, \quad \text{for } 10^4 < Re_b < 10^6 \qquad (3)$$

Substituting the present bulk Reynolds number, $Re_b = 1.6\times10^6$, in Eq. (3), it predicted a Nusselt number of 1.5×10^3. This Nusselt number corresponded to a heat transfer coefficient, h = 755. This value was also shown in Fig. 8 and it was larger than the computed h values at the downstream locations. The present computation indicated that, with combined hydraulic and thermal entry length, the circular duct flow had large thermal entry length. This is similar to the analysis of the thermal entry length with constant heat transfer rate.[16]

Square Duct Flow

Existing experiment[18] indicated that a developing turbulent square duct flow was fully developed at

$X/D \doteq 80$. For a fully developed square duct flow, analysis[17] showed that the averaged wall shear stress, $\bar{\tau}_w$, and the X-direction pressure gradient were related with

$$dp/dx = -4\bar{\tau}_w/D \tag{4}$$

Based on the experimental results of the averaged shear stress,[18] we used Eq. (4) to calculate the X-direction pressure gradient. The pressure gradient had a value of -0.045 lb/ft^2. This pressure gradient value was used as the downstream pressure boundary condition at $X/D = 80$ for the present computation. Some computational results of the duct center-line velocity, the skin friction factor and the surface heat transfer coefficient are described in the following.

The X-directional variations of the duct center-line velocity, U_c/U_∞, were plotted in Fig. 9. The computational results due to different grids and different turbulence models were compared with the existing experimental results.[19] All the results indicated that U_c/U_∞ increased to a large value at $X/D = 40$ and then U_c/U_∞ decreased slightly to a constant value at the downstream locations. The computational results showed a grid dependence when the Baldwin-Lomax eddy viscosity formula was used for turbulence modeling. The computation with $\beta_X = 1.1$ and $\beta_Y = \beta_Z = 1.0075$ predicted better the measured U_c/U_∞ valued than the computation with $\beta_X = 1.1$ and $\beta_Y = \beta_Z = 1.002$. With the Chien's turbulence model and $\beta_X = 1.1$ and $\beta_Y = \beta_Z = 1.0075$ grid in the computation, it could predict the measured U_c/U_∞ at most X/D locations. The computation did not predict better the measured U_c/U_∞ values than the computation with the Baldwin-Lomax eddy viscosity formula for turbulence modeling. Thus, the Baldwin-Lomax turbulence model was effective for the present computation to calculate the center-line velocity.

The computational results of the skin friction factor variations along the perimeter of the duct cross section at $X/D = 80$ were plotted in Fig. 10. The results with different grid configurations and different turbulence models were compared with existing experimental results.[18] These results indicated that C_f had a very small value at the corner location and the C_f value increased rapidly at the near corner locations ($Z/D < 0.1$) to a large value at $Z/D = 0.25$ location. The C_f value then remained approximately the same at the other peripheral locations. With the Baldwin-Lomax eddy viscosity formula and $\beta_X = 1.1$ and $\beta_Y = \beta_Z = 1.002$ grid, the computed C_f values agreed very well with the C_f measurements at all Z/D locations. With the Baldwin-Lomax eddy viscosity formula and $\beta_X = 1.1$ and $\beta_Y = \beta_Z = 1.0075$ grid in the computation, it calculated small friction factors at the near corner locations. With the Chien's turbulence model and $\beta_X = 1.1$ and $\beta_Y = \beta_Z = 1.0075$ grid in the computation, it computed high skin friction factors at all peripheral locations. With grid point packing at the near wall locations and the Baldwin-Lomax eddy viscosity formula for turbulence modeling, the computation could predict the experimental results of the skin friction factors.

The computational results of the surface heat transfer coefficients along the perimeter of the duct cross section at $X/D = 80$ were plotted in Fig. 11. The computational results due to different turbulence models or different computational grids were compared in this figure. The results indicated that very small heat transfer coefficients were calculated at corner locations. With the Baldwin-Lomax eddy viscosity formula and either one of the two different grids in the computation, it calculated approximately the same level of the surface heat transfer coefficients. With the Chien's k-ε turbulence model and $\beta_X = 1.1$, and $\beta_Y = \beta_Z = 1.0075$ grid in the computation, it calculated high surface heat transfer coefficients.

Circular to Rectangular Transition Duct

As it was previously described in the Computation section, the duct inlet was circular and the circular duct section was extended upstream to account for the actual wind tunnel inlet in the experiment.[6] A downstream static pressure, $p_d/p_\infty = 0.985$, was imposed at the downstream boundary of the domain of computation. The computation calculated a uniform static pressure ($p_u/p_\infty = 1.00$) at the duct inlet. The computed Mach number profile along the direction normal to the duct surface at $X/R = -2$ was plotted in Fig. 12. This Mach number profile was also compared with its experimental results.[1] The comparison showed good agreement between the results from the computation and the experiment. Some computational results of the surface pressure, the skin friction factor, and the heat transfer coefficient were described in the following sections.

The computational results of the static pressure variations along the top wall center line and the side wall center line were plotted in Fig. 13. The computational grid induced very small difference between the static pressures along the wall center lines. The difference is less than $0.01\ p_\infty$. Neglecting the grid effect on the static pressure computations, we could observe general trend of the static pressure variations along the wall center lines. Along the side wall center line locations, the pressure decreased and then increased within most part of the transition section. The pressure decreased rapidly within the downstream side of the transition section and the pressure maintained the same value along the side wall center line of the rectangular section. Along the top wall center line, the pressure increased and then decreased within most part of the transition section. The pressure increased rapidly at the end of the transition section and the pressure maintained the same value along the top wall center line of the rectangular section. The pressure levels were the same along the top wall center line and the side wall center line of the downstream rectangular section. Experiment[1] measured the pressure along the top wall center line. The measured values were plotted in Fig. 13 to verify the accuracy of the pressure computation. The computed pressure values were found to agree very well with their experimental values.

The computed skin friction factor, C_f, at locations along the top wall and the side wall center lines were shown in Fig. 14. The computational grids only induced difference in the predictions of the center-line C_f values within the upstream circular duct section. However, the C_f variation within the circular section was similar to the C_f variation of the developing circular duct flow (Fig. 7). The top wall center-line C_f values were the same as the side wall center-line C_f values. This trend was reversed within the upstream region of the transition section. In that region, the top wall center-line C_f values were lower than the side wall center-line C_f values. At the downstream locations, the top wall center-line C_f were higher than the side wall center-line C_f. Along the side wall center-line, C_f decreased to a small value and then increased within the transition section. The C_f values were approximately the same within the rectangular section. Along the top wall center-line, C_f decreased at the upstream locations of the transition section. Then C_f increased to a large value within the transition duct section. Again C_f decreased rapidly at locations near the end of the transition section. C_f maintained approximately the same values within rectangular section.

The surface heat transfer coefficient,

$$H = Q_w / (T_w - T_\infty) = -K dT/dn|_{n=0} / (T_w - T_\infty)$$

was computed at the locations along the top wall center line and the side wall center line. The computed surface heat transfer coefficients with the first grid in the computation were plotted in Fig. 15. In the computation, a step increase in the surface temperature boundary condition was imposed at X/R = –4 location (Fig. 4). At this location, H increased rapidly to a large value. H then decreased within the circular section and the H value at the side wall center line was about the same as the H values along the top wall center line. Along the side wall center line of the transition section, H decreased to a small value and then increased rapidly to a constant value within the rectangular section. Along the top wall center line, H increased at the upstream locations of the transition section. The H value then decreased slightly and maintained at a constant level at the downstream locations. In the rectangular section, the top wall center line had a larger H value than that of the side wall center line. Figure 16 showed the center line H values which were calculated with the 2nd grid in the computation. The computed H along the center lines were similar to the results (Fig. 16) when the 1st grid was used in the computation.

The experimental results[6] of the center-line heat transfer coefficients were plotted in Figs. 15 and 16 to verify the accuracy of the present heat transfer computation. The heat transfer coefficient of a fully developed turbulent circular duct flow[16] was also indicated in these figures. The computation predicted very well the experimental heat transfer coefficients at the end of the circular section. The heat transfer coefficients at X/R = 0 were very close to the H value of a fully developed turbulent circular duct flow. The present computation could predict the variation of the measured H value along the side wall center line. In the transition section, the computed top wall center line heat transfer coefficients were lower than the experimental H values. Using the 2nd grid in the computation, it improved the prediction of the top wall center-line heat transfer coefficients.

The computed H values at the locations along the perimeters of several duct cross sections were presented in a polar plot format in Fig. 17. Since the computation with the 2nd grid improved the prediction of the H values along the center line locations, the peripheral H variations due to 2nd grid in the computation were shown in Fig. 17. Some experimental H values were also plotted in this figure for comparisons with the computed H values. At X/R = –1, the duct had a circular cross section and the computation calculated approximately the same H values at all peripheral locations. The computed H values agreed well with their experimental values. At X/R = 0, the duct had a circular cross section and the computation predicted a decrease in the H values at large θ locations. The computational result of the H variation was similar to the result from the experiment. Within the transition section (at X/R = 1.0, 1.5 and 2), the computed H values decreased on the side wall surface and the H increased rapidly at the corner locations. The top wall surface H values were higher than the side wall surface H values. The computation could predict the experimental results of the peripheral heat transfer coefficient variation. The computed H values at all peripheral locations were large at the end of the transition duct section (X/R = 3.5) and the computation predicted accurately the experimental heat transfer coefficients at the top wall surface. The results in Fig. 17 also indicated that the transition section had large heat transfer coefficients at the duct corner locations. This observation was contrary to the results of the square duct computation which predicted very small heat transfer coefficients at the square duct corner locations. This could be due to the generation of the vortices at the transition duct corner locations.[1]

Summary

The objective of this research was to study the computation of the surface heat transfer coefficients of a transition duct flow. The transition duct flow had combined development of hydraulic and thermal entrance length. The axis of the transition duct was in line with the inlet flow direction. The inlet flow was subsonic (Mach number =0.34). The bulk Reynolds number was 1.6×10^6. The duct surface temperature was uniform. The duct cross section changed gradually from a circular shape at the upstream locations to a rectangular shape at the downstream locations.

The existing Proteus three-dimensional Navier-Stokes numerical computational code was used for the computations of the heat transfer coefficients. The Gridgen was used to generate the computational grids. Three major computational procedures were performed in this heat transfer study. The Navier-Stokes code was first used to compute the properties of the developing flows within a circular duct and a square duct. These computations served as the base-line verification of the effect of the computational grid, the Baldwin-Lomax eddy viscosity formula and the Chein's k-ε turbulence model on the computation. The code was then used to compute the surface heat transfer coefficients of the transition duct flow.

The present computation, with the Baldwin-Lomax eddy viscosity formula for turbulence modeling, predicted approximately the experimental results of the variations of the center-line velocity and the skin friction factor within the entrance region of a circular duct flow. The computation required grid point packing in the duct entrance in order to predict simultaneously the existing results of the center-line velocity, the skin friction factor and the surface heat transfer coefficient. The grid packing along the axial-direction had little effect on the prediction of the center-line velocity.

The square duct flow computation, with proper grid point packing and the Baldwin-Lomax eddy viscosity formula for turbulence modeling, predicted the measurements of the center-line velocity within the entrance region. With a few grid points in the near wall region, the computation also predicted the measurements of the skin friction factors along the perimeter of the downstream duct cross section. The computed surface heat transfer coefficients had very small values at the near corner locations. With the Chien's k-ε turbulence model in the computation, it improved the predictions of the center-line velocities at the downstream location and calculated large skin friction factors and the surface heat transfer coefficients at downstream locations.

The computations of the circular duct flow and the square duct flow indicated that the Baldwin-Lomax eddy viscosity formula was effective for turbulence modeling in the heat transfer computation. We only used this turbulence model in the transition duct computation. The computations were performed with two different grid configurations. The computation predicted the patterns of experimental surface heat transfer coefficient variations. The computed heat transfer coefficients at the upstream locations agreed very well with their experimental values and the computed heat transfer coefficients at the downstream locations were lower than their measurements. Different grid configuration induced small differences in the computational results of the surface pressure, the skin friction factor and the surface heat transfer coefficient. The computed surface heat transfer coefficients had large values at the locations near the corner of the downstream rectangular duct section.

The results in this report were obtained with the straight forward application of the existing Proteus three-dimensional Navier-Stokes computational code. The present computation used many default options of the numerical computational methods in the code. Some numerical schemes, such as the thin-layer option, various artificial viscosity models and different convergence criteria were not studied for their effects on the computations. The Proteus code provided great flexibility to specify the boundary conditions for the Navier-Stokes computations of an internal flow properties. We took the flexibility to specify the boundary conditions for the present computations. Theoretical analysis of the boundary conditions plays an important role in the numerical computations of subsonic flow properties. A detailed study of the transition duct flow boundary conditions is required to pursue further the flow computation. The present research considered only simple internal duct flows. The boundary conditions were derived from simple analyses and experimental results of the flow properties. The comparisons between the computed heat transfer coefficients and their measurements indicated that the Navier-Stokes computation could predict the heat transfer coefficients of a transition duct flow. The experience learned from the research was that a Navier-Stokes computation of the surface heat transfer rates of a transition duct, including the influence of boundary conditions, grid configuration and turbulence modeling, could be a formidable task.

References

1. Reichert, B.A., "A Study of High Speed Flows in an Aircraft Transition Duct," NASA TM–104449, 1991.
2. Davis, D.O., "Experimental Investigation of Turbulent Flow Through a Circular-to-Rectangular Transition Duct," NASA TM–105210, 1991.

3. Hippensteele, S.A., Russell, L.M, and Stepka, F.S., "Evaluation of a Method for Heat Transfer Measurements and Thermal Visualization Using a Composite of a Heater Element and Liquid Crystals," NASA TM–81639, 1981.
4. Hippensteele, S.A., Russell, L.M., and Torres, F.J., "Local Heat-Transfer Measurements on a Large Scale-Model Turbine Blade Airfoil Using a Composite of a Heater Element and Liquid Crystals," Journal of Engineering for Gas Turbines and Power, Vol. 107, Oct. 1985, pp. 953–960.
5. Jones, T.V., and Hippensteele, S.A., "High-Resolution Heat-Transfer-Coefficient Maps Applicable to Compound-Curve Surface Using Liquid Crystals in a Transient Wind Tunnel," NASA TM–89855, 1988.
6. Hippensteele, S.A., and Poinsatte, P.E., "Transient Liquid-Crystal Technique Used to Produce High-Resolution Convective Heat-Transfer-Coefficient Maps for a Super-Elliptic Transition Duct," Under preparation for a NASA Technical Report.
7. Steinbrenner, J.P., and Chawner, C.L.F., "The Gridgen 3D Multiple Block Grid Generation System," 1991.
8. Wilcox, D.C., "Turbulence Modeling for CFD," Published by DCW Industries, Inc., 1993.
9. Towne, C.E., Schwab, J.R., and Trong, T.B., "Proteus Three-Dimensional Navier-Stokes Computer Code-Version 1.0, Volume 1-Analysis Description," NASA TM–106337, 1993.
10. Towne, C.E., Schwab, J.R., and Trong, T.B., "Proteus Three-Dimensional Navier-Stokes Computer Code-Version 1.0, Volume 2-User's Guide," NASA TM–106340, 1993
11. Towne, C.E., Schwab, J.R., and Trong, T.B., "Proteus Three-Dimensional Navier-Stokes Computer Code-Version 1.0, Volume 3-Programmer's Reference," NASA TM–106341, 1993.
12. Baldwin, B.S., and Lomax, H., "Thin Layer Approximation and Algebraic Model for Separated Turbulent Flows," AIAA Paper 78–257, 1978.
13. Chien, K.Y., "Prediction of Channel and Boundary-Layer Flows with a Low-Reynolds-Number Turbulence Model," AIAA Journal, Vol. 20, No. 1, 1982, pp. 33–38.
14. Beam, R.M., and Warming, R.F., "An Implicit Factored Scheme for the Compressible Navier-Stokes Equations," AIAA Journal, Vol. 16, No. 4, 1978, pp. 393–402.
15. Briley, W.R., and McDonald, H., "Solution of the Multidimensional Compressible Navier-Stokes Equations by a Generalized Implicit Method," Journal of Computational Physics, Vol. 24, 1977, pp. 373–397.
16. Kays, W.M., "Convective Heat and Mass Transfer," McGraw-Hill, 1966, p. 173.
17. Ward-Smith, A.J., " Internal Fluid Flow," Clarendon Press, Oxford, 1980, pp. 247–249.
18. Gessner, F.B., Eppich, H.M., and Lund, E.G., "Reynolds Number Effects on the Near-Wall Structure of Turbulent Flow Along a Streamwise Corner," Near-Wall Turbulent Flows, Elsevier, 1993, pp. 965–975.
19. Gessner, F.B., and Emery, A.F., "The Numerical Prediction of Developing Turbulent Flow in Rectangular Ducts," In Turbulent Shear Flow 2, Springer, 1980.

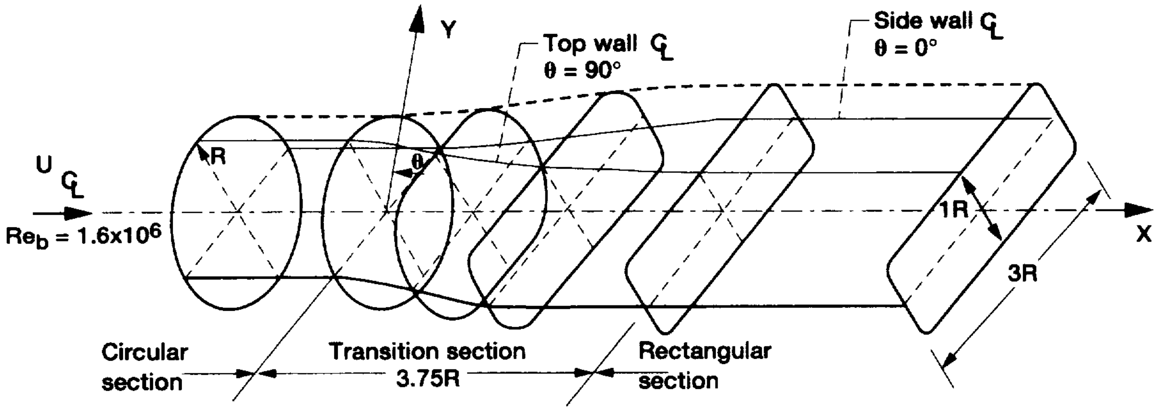

Figure 1.—Circular to rectangular transition duct.

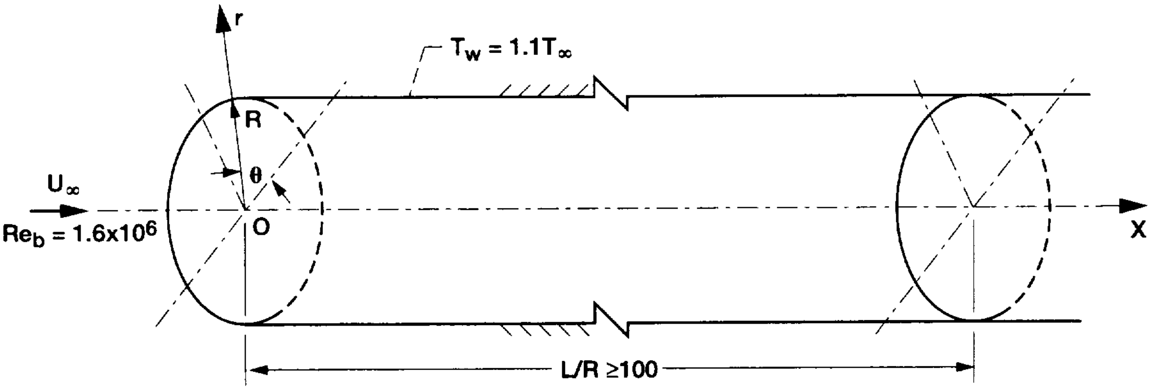

Figure 2.—Circular duct.

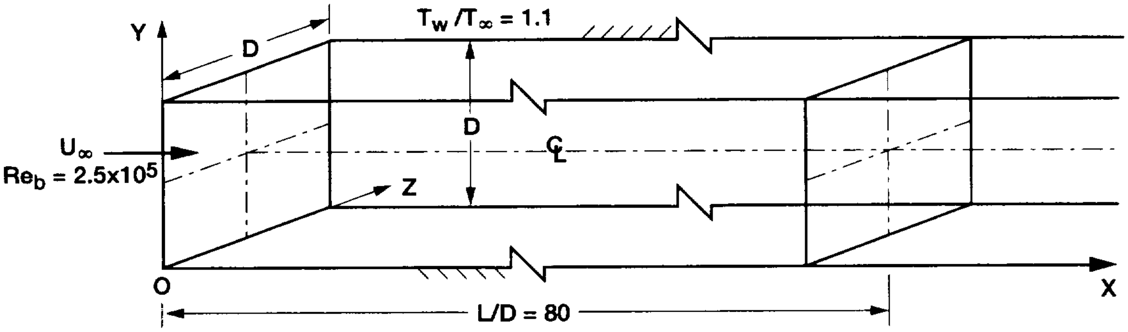

Figure 3.—Square duct.

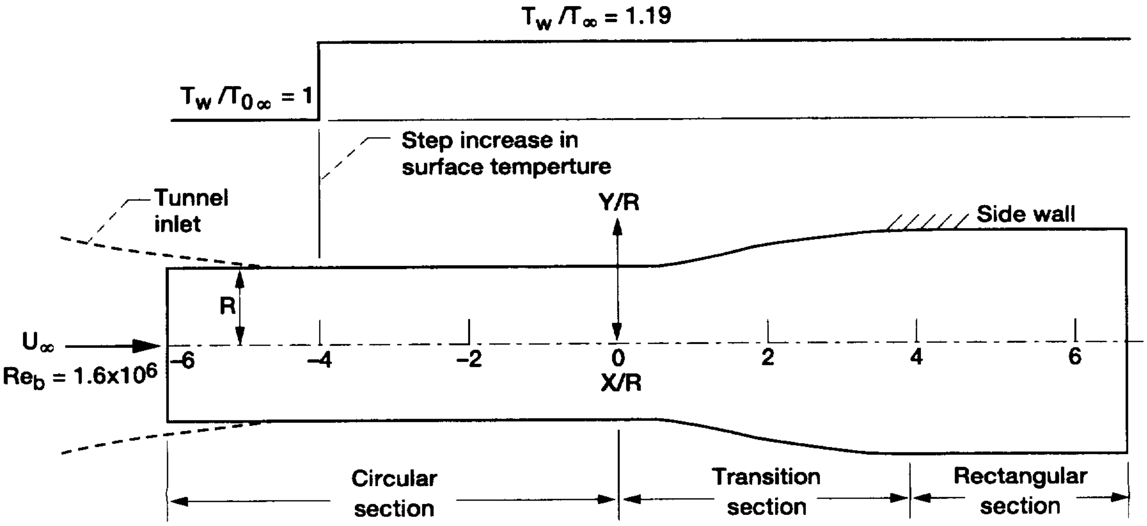

Figure 4.—Circular to rectangular duct for computation.

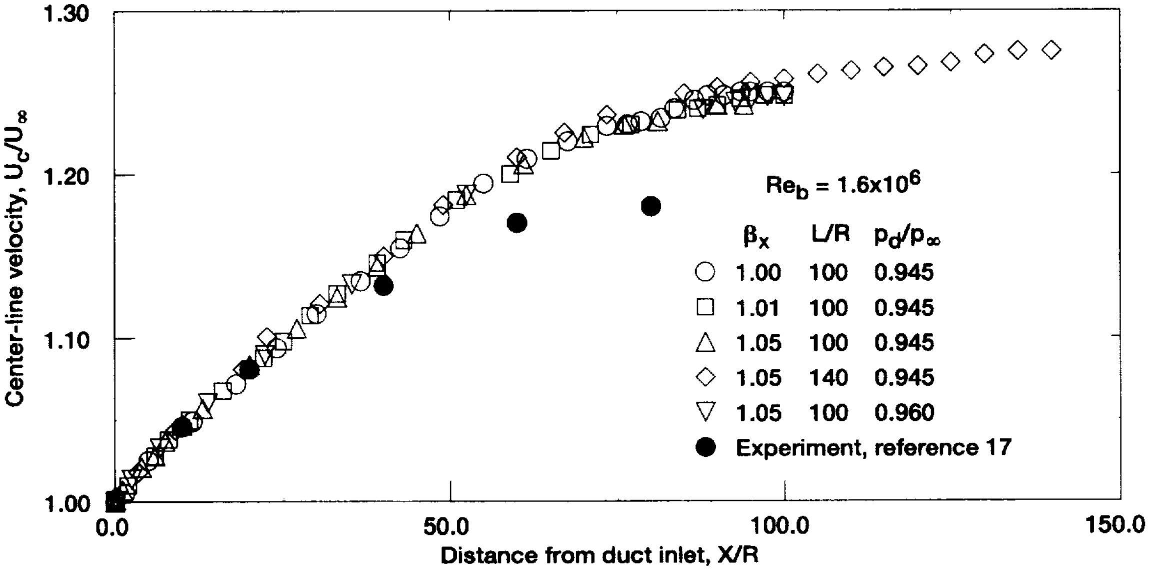

Figure 5.—Comparisons of circular duct center-line velocities.

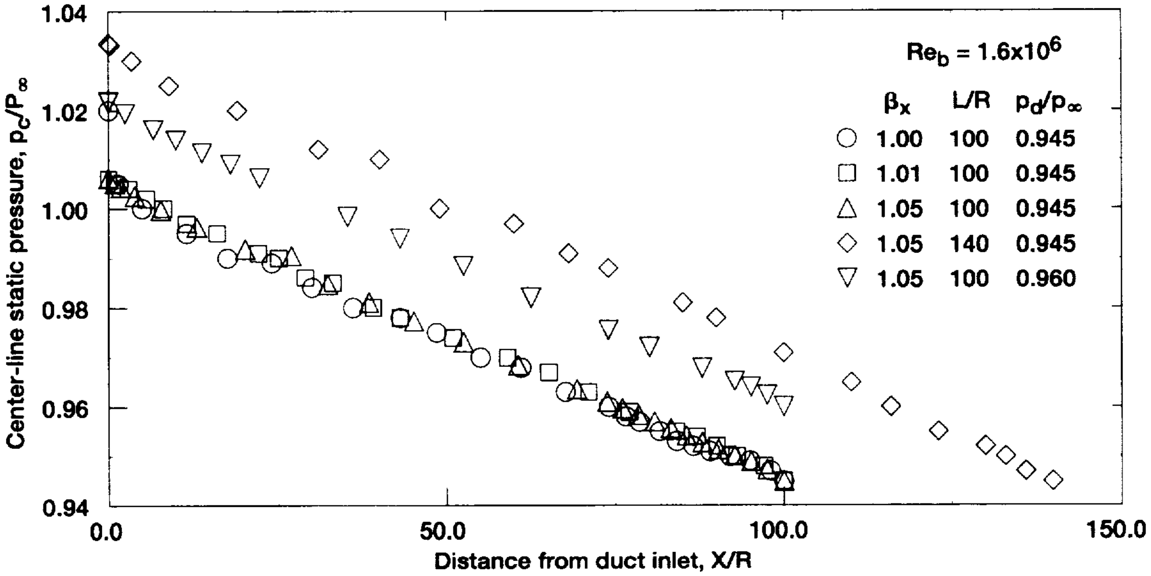

Figure 6.—Static pressure variations along circular duct center line.

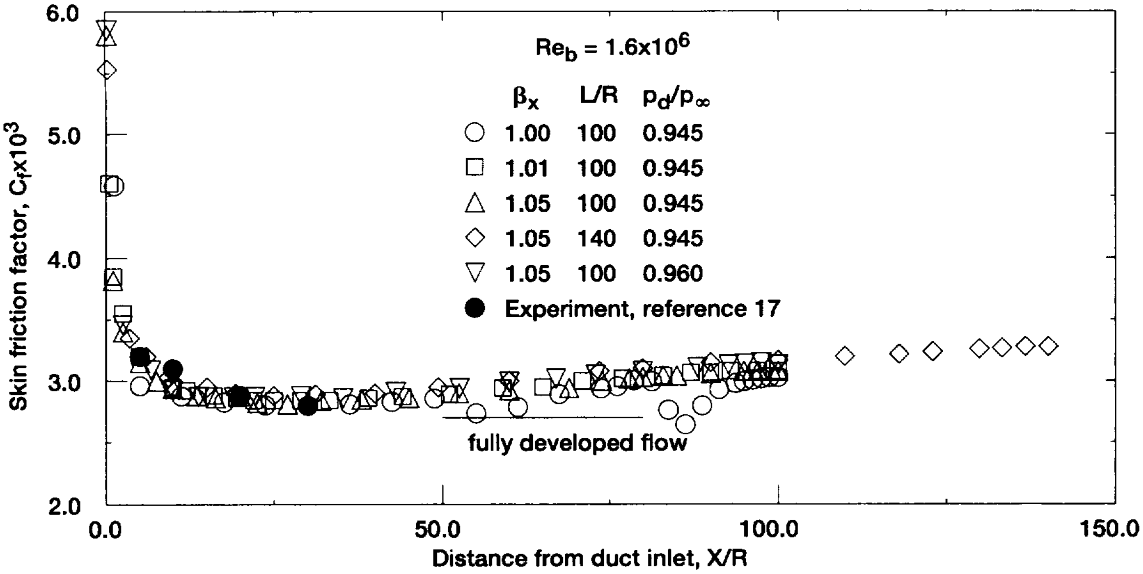

Figure 7.—Skin friction factors of circular duct flow.

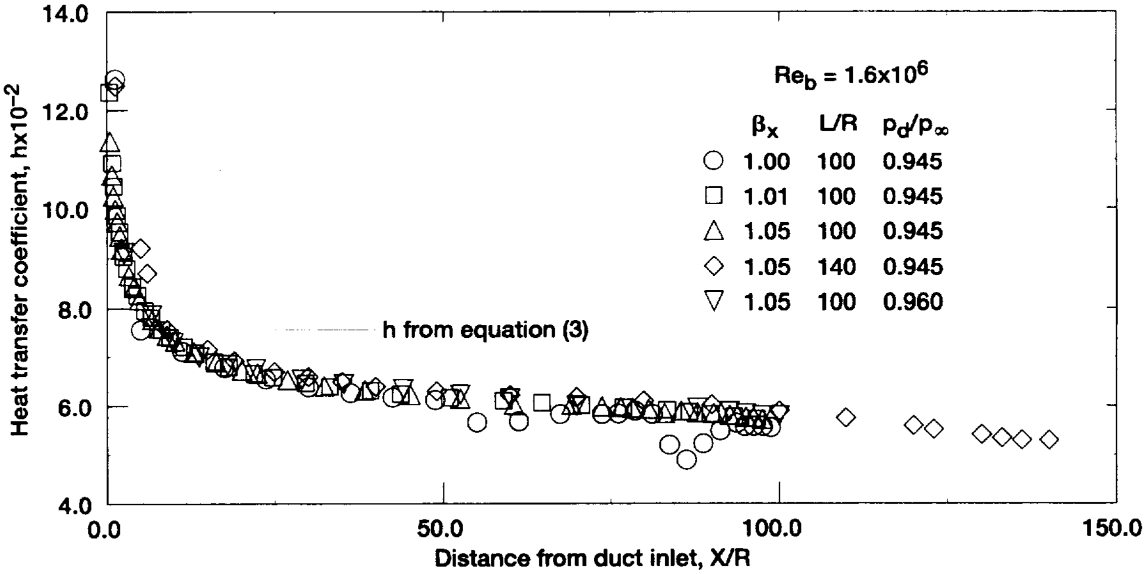

Figure 8.—Heat transfer coefficients of circular duct flow.

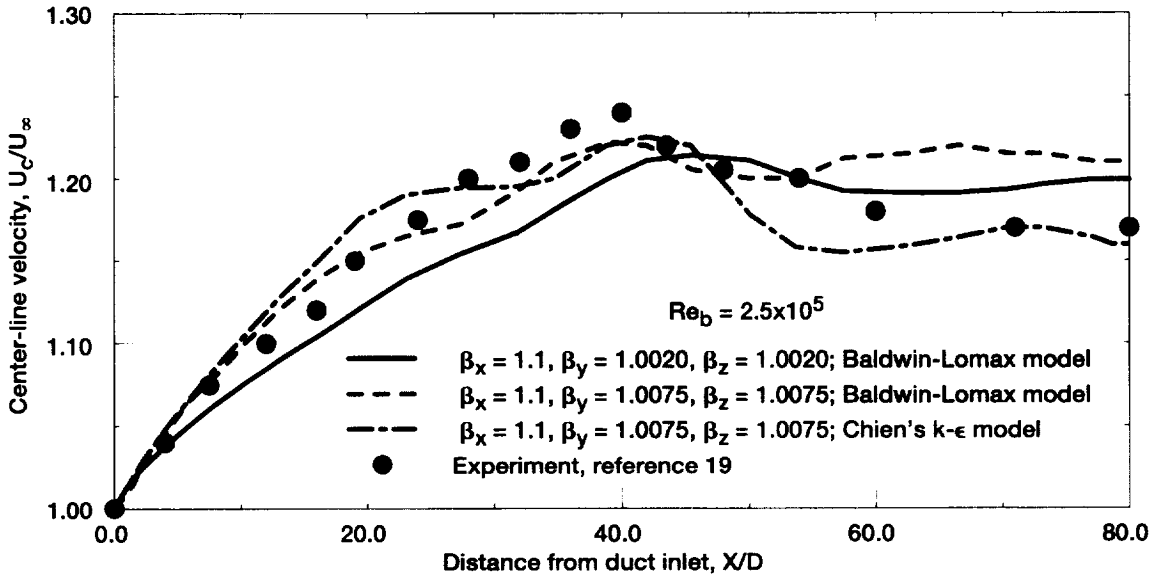

Figure 9.—Comparisons of square duct center-line velocities.

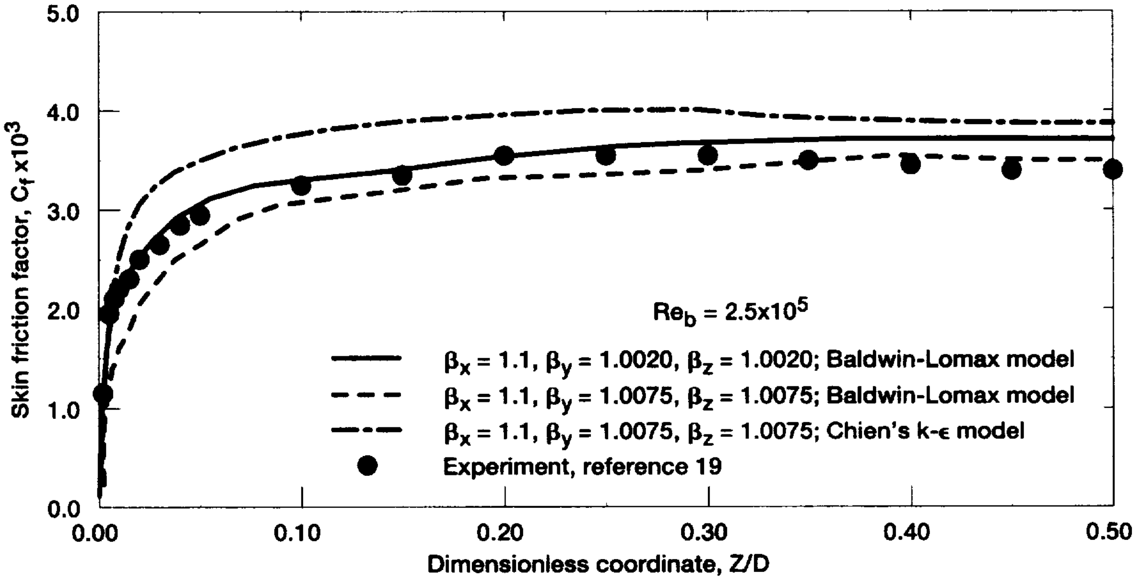

Figure 10.—Comparisons of square duct skin friction factors.

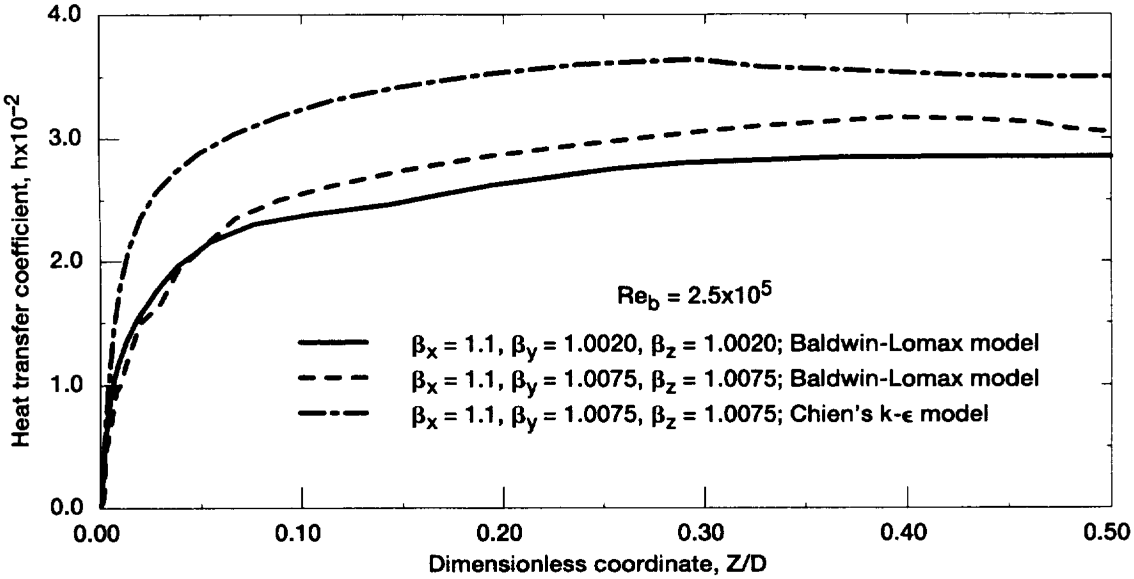

Figure 11.—Comparisons of square duct heat transfer coefficients.

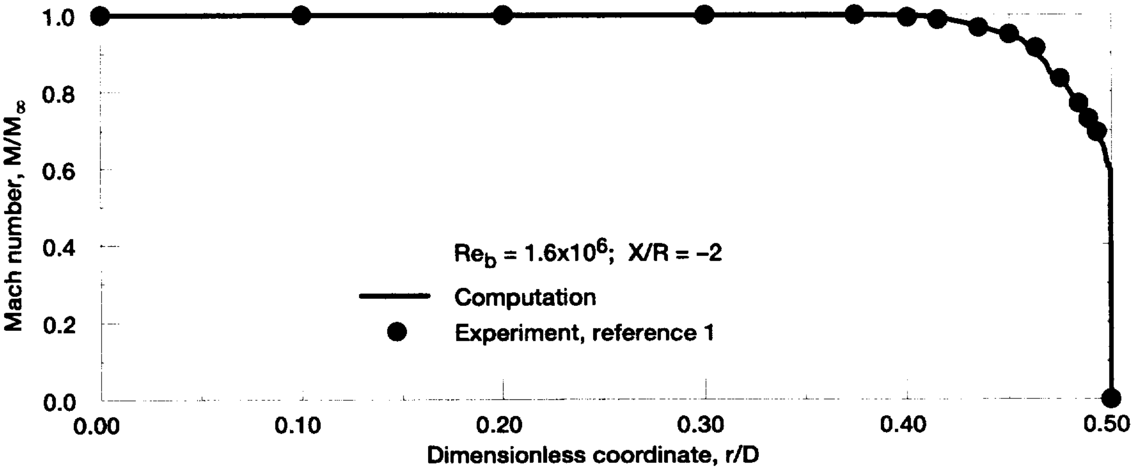

Figure 12.—Comparison of upstream Mach number profiles.

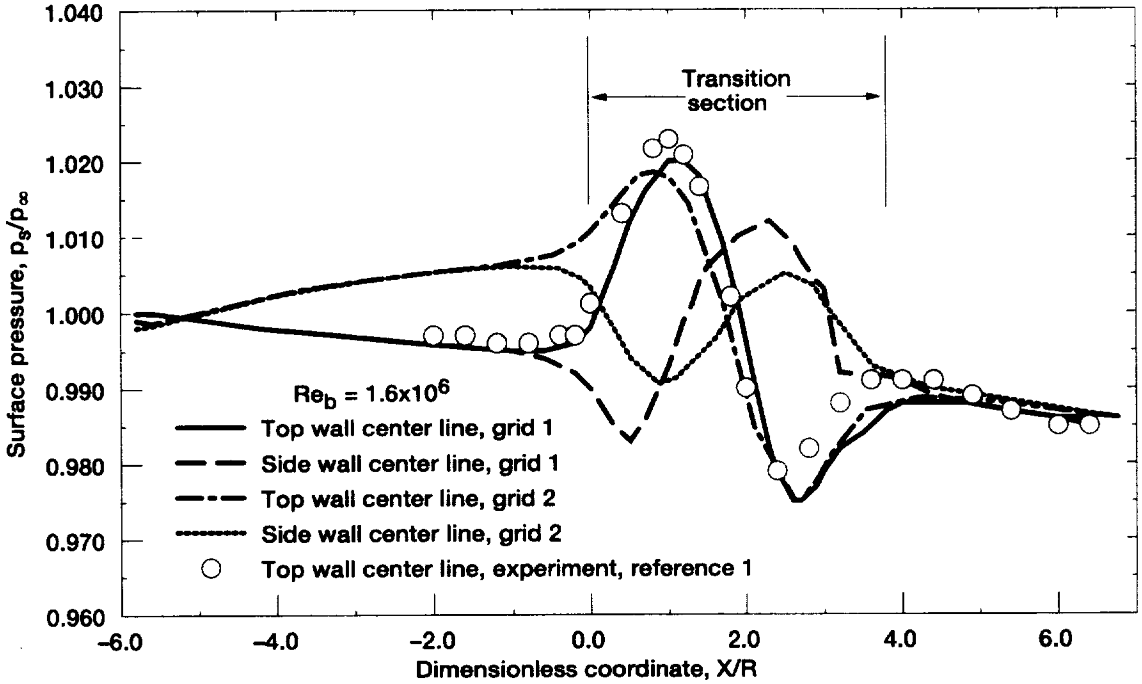

Figure 13.–Surface pressure along transition duct wall center lines.

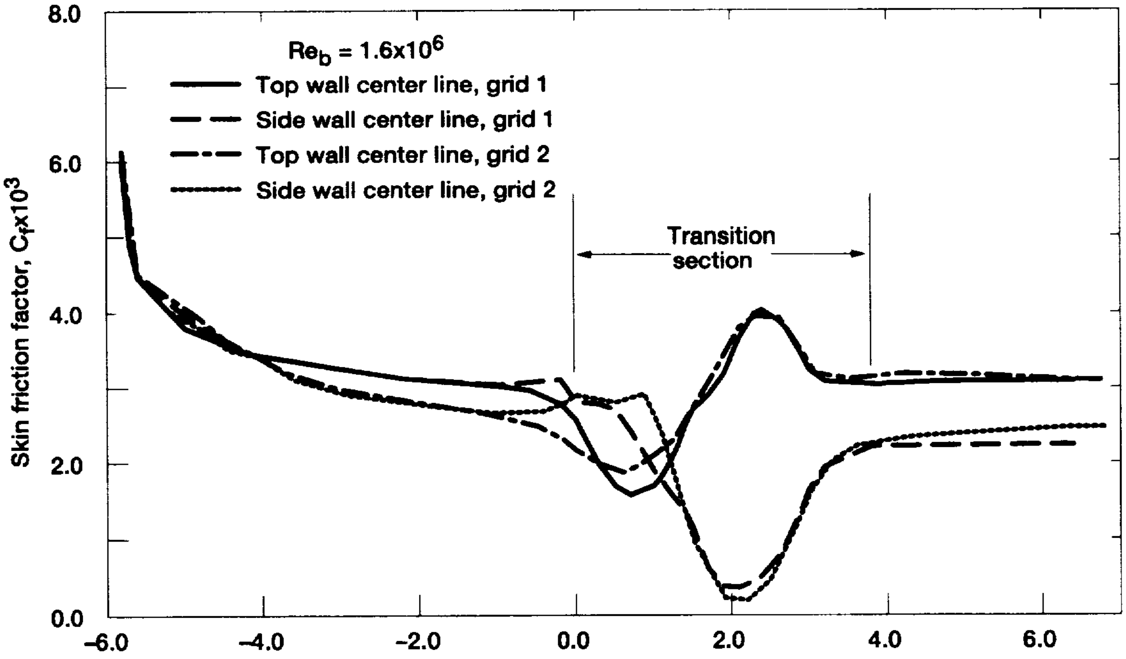

Figure 14.—Skin friction factors along transition duct wall center lines.

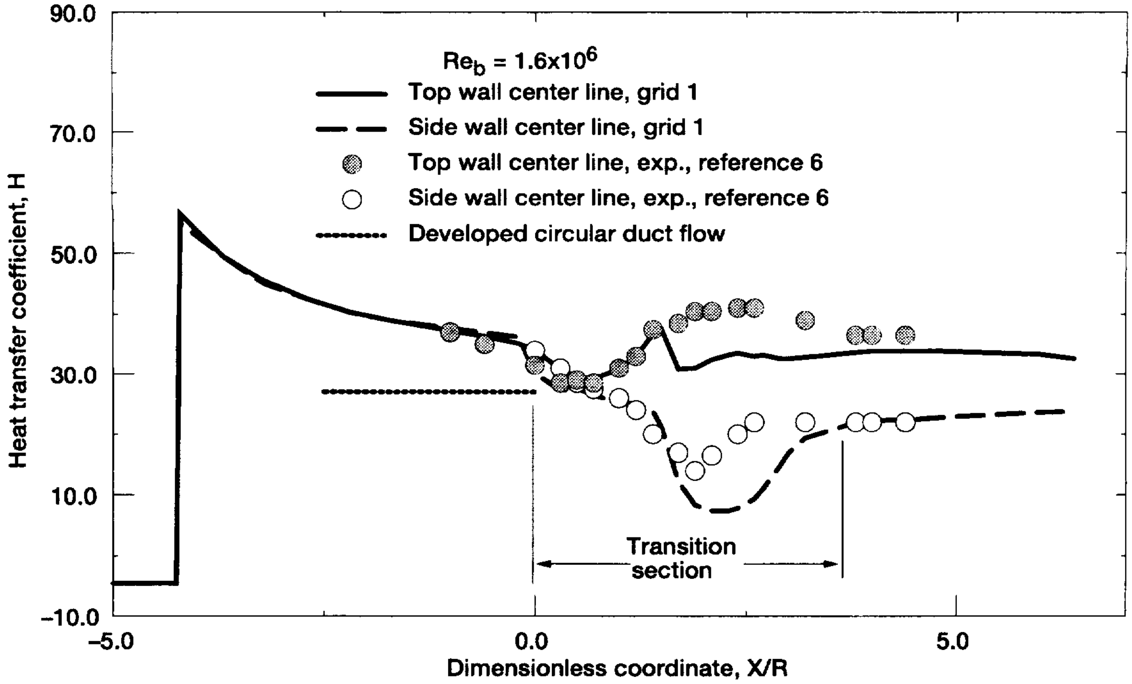

Figure 15.—Heat transfer coefficients along transition duct wall center lines.

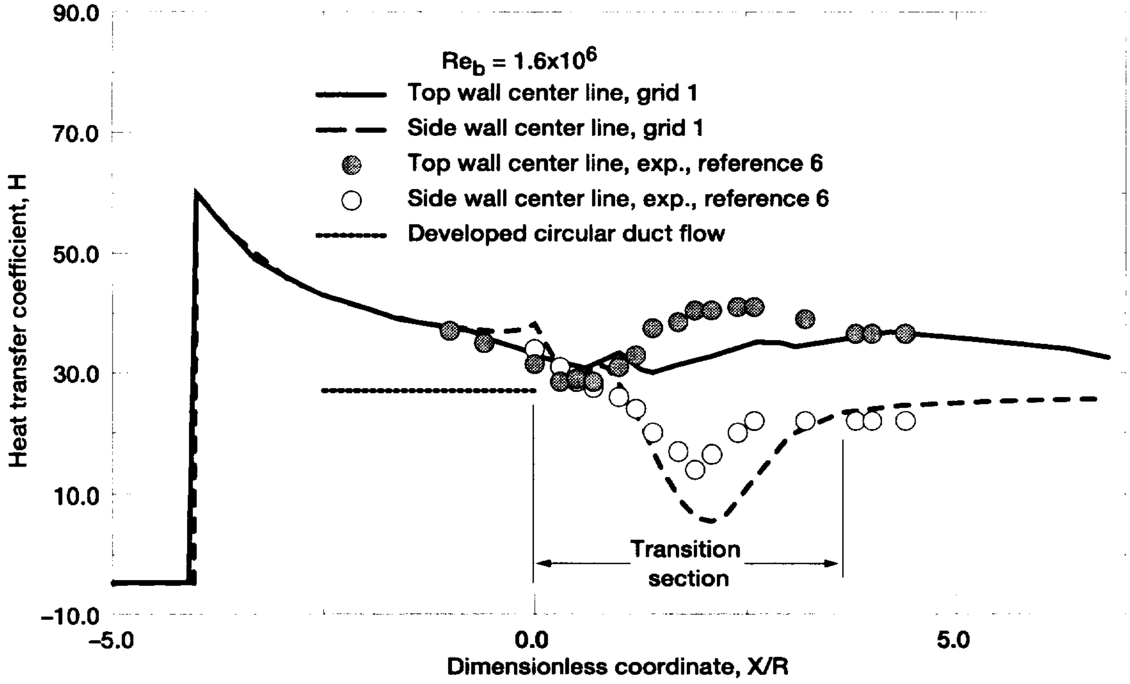

Figure 16.—Heat transfer coefficients along transition duct wall center lines.

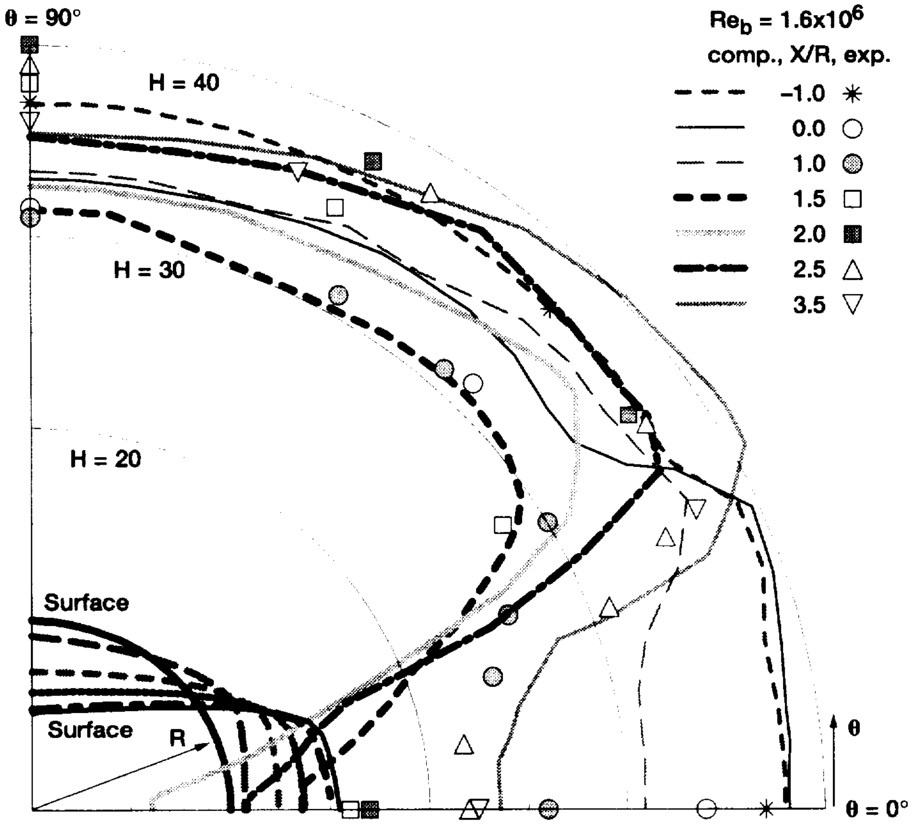

Figure 17.—Heat transfer coefficients along transition duct cross sections.

REPORT DOCUMENTATION PAGE

Form Approved
OMB No. 0704-0188

1. AGENCY USE ONLY (*Leave blank*)	**2. REPORT DATE** May 1997	**3. REPORT TYPE AND DATES COVERED** Technical Memorandum

4. TITLE AND SUBTITLE

Heat Transfer Computations of Internal Duct Flows With Combined Hydraulic and Thermal Developing Length

5. FUNDING NUMBERS

WU–523–26–13

6. AUTHOR(S)

C.R. Wang, C.E. Towne, S.A. Hippensteele, and P.E. Poinsatte

7. PERFORMING ORGANIZATION NAME(S) AND ADDRESS(ES)

National Aeronautics and Space Administration
Lewis Research Center
Cleveland, Ohio 44135–3191

8. PERFORMING ORGANIZATION REPORT NUMBER

E–10731

9. SPONSORING/MONITORING AGENCY NAME(S) AND ADDRESS(ES)

National Aeronautics and Space Administration
Washington, DC 20546–0001

10. SPONSORING/MONITORING AGENCY REPORT NUMBER

NASA TM–107450
AIAA–97–2486

11. SUPPLEMENTARY NOTES

Prepared for the 32nd Thermophysics Conference sponsored by the American Institute of Aeronautics and Astronautics, Atlanta, Georgia, June 23–25, 1997. Responsible person, C.R. Wang, organization code 5820, (216) 433–5865.

12a. DISTRIBUTION/AVAILABILITY STATEMENT

Unclassified - Unlimited
Subject Category 07

This publication is available from the NASA Center for AeroSpace Information, (301) 621–0390.

12b. DISTRIBUTION CODE

13. ABSTRACT ***(Maximum 200 words)***

This study investigated the Navier-Stokes computations of the surface heat transfer coefficients of a transition duct flow. A transition duct from an axisymmetric cross section to a nonaxisymmetric cross section, is usually used to connect the turbine exit to the nozzle. As the gas turbine inlet temperature increases, the transition duct is subjected to the high temperature at the gas turbine exit. The transition duct flow has combined development of hydraulic and thermal entry length. The design of the transition duct required accurate surface heat transfer coefficients. The Navier-Stokes computational method could be used to predict the surface heat transfer coefficients of a transition duct flow. The Proteus three-dimensional Navier-Stokes numerical computational code was used in this study. The code was first studied for the computations of the turbulent developing flow properties within a circular duct and a square duct. The code was then used to compute the turbulent flow properties of a transition duct flow. The computational results of the surface pressure, the skin friction factor, and the surface heat transfer coefficient were described and compared with their values obtained from theoretical analyses or experiments. The comparison showed that the Navier-Stokes computation could predict approximately the surface heat transfer coefficients of a transition duct flow.

14. SUBJECT TERMS

Heat transfer; Internal duct flow; Navier-Stokes computation

15. NUMBER OF PAGES

20

16. PRICE CODE

A03

17. SECURITY CLASSIFICATION OF REPORT Unclassified	**18. SECURITY CLASSIFICATION OF THIS PAGE** Unclassified	**19. SECURITY CLASSIFICATION OF ABSTRACT** Unclassified	**20. LIMITATION OF ABSTRACT**

NSN 7540-01-280-5500

Standard Form 298 (Rev. 2-89)
Prescribed by ANSI Std. Z39-18
298-102